RSC Advances

ROYAL SOCIETY OF CHEMISTRY

www.rsc.org/advances

Graphical abstract

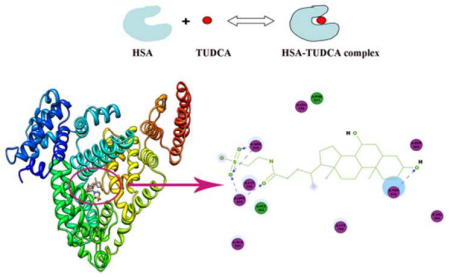

Binding patterns and structure-affinity relationship of tauroursodeoxycholic acid with human serum albumin were established by NMR methodology and docking simulations.

Binding mechanism of tauroursodeoxycholic acid to human serum albumin: insights from NMR relaxation and docking simulations

Di Wu [a], Yuanming Zhai [b], Jin Yan [a], Kailin Xu [a], Qing Wang [a], Yuanzhi Li[a], and Hui Li [a, *]

[a] *College of Chemical Engineering, Sichuan University, Chengdu 610065, P. R. China*

[b] *Analytical & Testing Center Sichuan University, Chengdu 610064, P. R. China*

* Corresponding author.

Address: College of Chemical Engineering, Sichuan University, Chengdu 610065, China.

Tel.: +86 028 85405149; *Fax:* +86 028 85401207.

E-mail address: lihuilab@sina.com(Hui Li)

Abstract:

The binding mechanism of drugs with human serum albumin (HSA) is one of the most important factors in monitoring drug concentration in the blood and its transport to the destination tissues. The binding interaction of HSA with tauroursodeoxycholic acid (TUDCA), an endogenous bile acid, was investigated at molecular level through NMR methodology. This methodology was based on the analysis of the selective and non-selective spin–lattice relaxation rate changes in ligand protons, affinity index, and molecular dynamic simulations to understand the binding strength and physical–chemistry information on the interaction between HSA and the drug used in therapy. Results showed that TUDCA could strongly bind to HSA in site 1. The binding mode was further analysed using AutoDock. This study

provided new insights into the interaction mechanism of TUDCA and HSA.

1. Introdution

Studies on the interactions between drugs and biological macromolecules have been objects of interest in therapeutic drug monitoring, and have significantly contributed to understanding of the physicochemical mechanism and several biological and behavioral activities of drugs transported in human bodies. By binding to human serum albumin (HSA), the most abundant protein in the circulatory system, several exogenous and endogenous substances circulate in the plasma.[1, 2] HSA is a globular protein composed of three homologous helical domains (I–III). Each domain consists of two subdomains (A and B) containing 585 amino acid residues and stabilized by 17 disulfide bridges.[3] The principal binding regions on HSA are located in subdomains IIA (Sudlow's site 1) and IIIA (Sudlow's site 2).[4] Under natural conditions, the overall structure of HSA is flexible during ligand binding. Given its exceptional abilities, HSA is commonly used as a model protein for biophysical and physicochemical studies. It is widely accepted that the degree of affinity between HSA and drugs can dominate their distribution into target tissues, affect their elimination, and influence their therapeutic or toxic effects.[5]

Tauroursodeoxycholic acid (TUDCA) (Fig.1), an endogenous hydrophilic bile acid normally produced at very low levels in humans and a commercially available bile acid derivative, is widely used to treat cholelithiasis and cholestatic liver disease.[6-9] An increasing number of

detail pharmacological effects of TUDCA were reported, which demonstrated that TUDCA possesses potential therapeutic strategy for the prevention and treatment of many diseases and already attracted widespread attention of relative scholars. TUDCA has a unique role in modulating cell death by interrupting the classic pathways of apoptosis.[10] Several studies have demonstrated that TUDCA serves as an anti-apoptotic agent for a number of neurodegenerative diseases, including amyotrophic lateral sclerosis, Alzheimer's disease, Parkinson's disease, and Huntington's disease.[11] TUDCA can also serve as a chemical chaperone to inhibit oxygen-radical production,[12] reduce endoplasmic reticulum stress,[13] and stabilize unfolded protein response.[14] However, limited reports are available describing the transporters involved in the disposition of TUDCA in its drug-protein interactions.

Several methods have been utilized to determine the interaction parameters between drugs and proteins, such as equilibrium dialysis,[15,16] isothermal titration calorimetry,[17,18] capillary electrophoresis,[19,20] and spectroscopic analysis (fluorescence, ultraviolet visible absorption, circular dichroism, and Fourier transform infrared spectroscopy).[21-25] Another technique used for the system is nuclear magnetic resonance (NMR), which allows the analysis of biological systems in real time under its working conditions.[26,27] In the present study, a NMR methodology based on the quantitative analysis of selective and non-selective spin-lattice relaxation rate changes in TUDCA proton and the affinity index was utilized to confirm the formation and dynamic properties of the TUDCA-HSA complex and their binding affinities. Complementarily, we performed molecular dynamic (MD) simulations to determine the orientation of the TUDCA molecule on HSA for visualization of the binding properties.

Overall, the present study will provide interesting insights for drug-protein interactions.

2. Materials and methods

2.1 Reagents and Chemicals

Essential fatty acid free HSA was purchased from Sigma-Aldrich (Milwaukee, USA) and used without further purification. Deuterium oxide at 99.9% purity was provided by Cambridge Isotope Lab (Germany). The HSA stock solutions were prepared in 30 mM sodium phosphate buffer solution using deuterated water at pH 7.4 (uncorrected for D_2O) and stored in the dark at 4 °C. TUDCA was purchased from Aladdin Chemical Reagent (Shanghai, China). All other reagents were of analytical grade.

2.2 NMR methods

NMR spectroscopy was utilized to measure the proton spin relaxation rate based on the comparison of the non-selective (R^{ns}) and selective (R^{se}) spin–lattice relaxation rates in the presence and absence of a macromolecule receptor. The R^{ns} and R^{se} are defined by the following equations:

$$R_i^{ns} = \sum_{j \neq i} \rho_{ij} + \sum_{j \neq i} \sigma^{ij} \quad (1)$$

$$R_i^{se} = \sum_{j \neq i} \rho_{ij} \quad (2)$$

Thus,

$$R_i^{ns} = R_i^{se} + \sum_{j \neq i} \sigma^{ij} \quad (3)$$

Where ρ_{ij} and σ^{ij} are the self-relaxation and cross-relaxation rates for any H_i-H_j interaction and the sum is expend to all dipolar connected protons.

The explicit forms of R_i^{ns} and R_i^{se} are as follows:

$$R_i^{ns} = \frac{1}{10}\frac{\gamma_H^4\hbar^2}{r_{ij}^6}\left[\frac{3\tau_c}{1+\omega_H^2\tau_c^2}+\frac{12\tau_c}{1+4\omega_H^2\tau_c^2}\right] \quad (4)$$

$$R_i^{se} = \frac{1}{10}\frac{\gamma_H^4\hbar^2}{r_{ij}^6}\left[\frac{3\tau_c}{1+\omega_H^2\tau_c^2}+\frac{6\tau_c}{1+4\omega_H^2\tau_c^2}+\tau_c\right] \quad (5)$$

The formation of a ligand–receptor complex affects R_i^{ns} and R_i^{se} depending on the dynamical parameters such as the molecular rotational correlation time τ_c, at different extents. For instance, $R_i^{ns} < R_i^{se}$ when it is at the fast molecular reorientation time regime, which is typical for a free ligand ($\omega_H\tau_c \ll 1$). $R_i^{ns} < R_i^{se}$ when it is at slow motion, which is typical for a ligand bound to a macromolecule ($\omega_H\tau_c \gg 1$).[28-32]

Under the condition of a fast chemical exchange between the free and bound environments, the experimentally observed selective relaxation R_i^{se} can be expressed by the following equation:

$$R_{iobs}^{se} = X_f R_{if}^{se} + X_b R_{ib}^{se} \quad (6)$$

where R_{iobs}^{se} is the experimentally determined selective relaxation rate. R_{if}^{se}, X_f, R_{ib}^{se}, and X_b are the selective spin–lattice relaxation rates and the ligand fractions in free and bound states, respectively. Considering the ligand–receptor equilibrium:

$$M + L = ML \quad (7)$$

with a thermodynamic equilibrium constant $K = [ML]/[M][L]$. Assuming $[L] \gg [M_0]$, then:

$$\Delta R_i^{se} = \frac{KR_{ib}^{se}}{1+K[L]}[M_0] \quad (8)$$

where $\Delta R_i^{se} = R_{iobs}^{se} - R_{if}^{se}$ and $[M_0]$ is the initial concentration of the macromolecule. According to Eq. (8), the plot of ΔR_i^{se} versus $[M_0]$ would result in a straight line, with slope $[A]_L^T$:

$$[A]_L^T = \frac{KR_{ib}^{se}}{1+K[L]} \tag{9}$$

defined as the "affinity index" (L mol^{-1} s^{-1}).[33] This parameter is constant at fixed temperature and ligand concentration, and can be used to gain insights into the dynamics of the ligand–receptor interaction to understand the strength.[34]

Considering the differences in the dynamics of the portions of the molecule caused by different correlation times and modulating the dipolar interactions between protons at different positions, that affect selective relaxation rates, the affinity index must be normalized to the relaxation rate of the free ligand. The normalization of $\Delta R_i^{se} = R_{iobs}^{se} - R_{if}^{se}$ to R_{if}^{se} removes the above-mentioned factors, leading to a normalized affinity index:[35]

$$\Delta R_{iN}^{se} = \frac{KR_{ib}^{se}}{(1+K[L])R_{if}^{se}}[M_0] \tag{10}$$

The dependence of the normalized relaxation rate enhancements ΔR_{iN}^{se} from the concentration of the macromolecule $[M_0]$ is represented by a straight line passing through the origin of the axes with slope:

$$[A_i^N]_L^T = \frac{KR_{ib}^{se}}{(1+K[L])R_{if}^{se}} \tag{11}$$

$[A_i^N]_L^T$ is defined as the "normalized affinity index" (mol^{-1} L) and remains constant at a specified temperature and ligand concentration.[26,36] Furthermore, Eq. 10 can be rewritten as:

$$\frac{1}{\Delta R_{iN}^{se}} = \frac{(1 + K[L])R_{if}^{se}}{KR_{ib}^{se}[M_0]} \quad (12)$$

$$\frac{1}{\Delta R_{iN}^{se}} = \frac{R_{if}^{se}}{KR_{ib}^{se}[M_0]} + \frac{[L]R_{if}^{se}}{R_{ib}^{se}[M_0]} \quad (13)$$

analysis of $1/\Delta R_{iN}^{se}$ in relation to ligand concentration should observe the complex equilibrium constant *K*.

2.3 NMR measurements

All measurements were performed using a Bruker Avance 400 MHz NMR spectrometer operating at 400.13 MHz for hydrogen at 25 °C. The spin–lattice relaxation rates were measured using the (180°–τ–90°–*t*) sequence. The τ values used for the selective and non-selective experiments were 0.01, 0.2, 0.2, 0.3, 0.4, 0.5, 0.6, 0.7, 0.8, 1, 1.2, 1.5, 2, 3, and 5.0 s. The delay time *t* in this case was 5 s. The 180° selective inversion of the proton spin population was obtained through a selective soft Gaussian perturbation pulse (width: 20 ms, power: 60 dB) corresponding to an excitation width of about 45 Hz. The solutions for the NMR experiments were prepared by dissolving appropriate amounts of TUDCA and HSA in 99.9% D_2O and 30 mM phosphate buffer, at pH 7.4, respectively, and then a stream of dry argon was passed through to degas the solutions. In all experiments the ligand TUDCA concentration was 4.0 mM. Moreover, the HSA concentrations used to obtain the affinity index were 0, 3.0, 6.0, 9.0, 12, and 15 μmol. The formation of the ligand–protein complex mainly affected the observed R_i^{se} enhancements because the addition of HSA did not change the viscosity of the system.[37]

Generally, considering that the recovery of the proton longitudinal magnetization after a 180°

pulse is not a single exponential because of the sum of different relaxation terms, the selective spin–lattice relaxation rates were calculated using the initial slope approximation and a subsequent three parameter exponential regression analysis of the longitudinal recovery curves.[35] The affinity parameters were calculated through a linear regression analysis of the experimental data. The maximum experimental error in the measurements was 5%. All NMR data processing and analyses were performed using Topspin 2.1 software (Bruker BioSpin Ltd.).

2.4 Molecular docking

All docking simulations were performed using AutoDock Version 4.2.5.1 program package and AutoDock Tools (ADT) Version 1.5.6 to identify the potential ligand binding sites. Lamarckian genetic algorithm (LGA) implemented in AutoDock was applied to estimate the possible conformations of the ligand-protein complex. The available HSA crystal structure used in the docking studies was obtained from the RCSB Protein Data Bank (PDB ID: 1H9Z). The receptor (HSA) and ligand (TUDCA) were pretreated. For the receptor preparation, water molecules were removed, polar hydrogen atoms were added, and Kollman united atom partial charges were assigned to HSA using ADT at a desired pH of 7.4. For the ligand preparation, the 3D structure was generated with the use of ChemBioOffice Version 11.0 and optimized using the Austin model-1 (AM1) method.[38] To recognition of the all binding sites in HSA, docking was performed by setting the grid box size at 126 Å×126 Å×126 Å along the x, y, and z axes, thereby covering the whole protein with a grid spacing of 0.697 Å. AutoGrid was then run to generate the grid map of the various ligand and receptor atoms. After the grid map

was generated, ligand flexible docking simulations were performed with 300 runs and 2.5 × 10^6 energy evaluations, 27000 generations and genetic algorithm population of 200 individuals. In addition, cluster analysis was performed on the docked results. Subsequently, smaller grid maps were defined using 70 Å×80 Å×70 Å points with a grid spacing of 0.503 Å centered at the coordinates x= 25.005, y= 10.344, and z= 8.468. A subsequent round of dockings with the number of independent runs set to 200 was performed to locate the optimum binding site. The result with the lowest docking energy analysis in cluster rank 1 was used for further analysis. For visualization of the docked conformations, Discovery studio 3.1 (State Key Laboratory of Biotherapy, Sichuan University, China) software package was used.

3 Results and discussion

Fig. 2 shows the ^{1}H spectrum of TUDCA in D_2O solution at 400 MHz with the resonance assignments. The poor signal/noise ratio increased the errors. The proton NMR of TUDCA was fully assigned and accorded with the literature.[39] Detailed ^{1}H chemical shift values of TUDCA are summarized in Table 1. As overlapping peaks were not appropriate for 180° shape pulse to get right selective relaxation rate, the signal allowed for the observation of changes and selected for the selective and non-selective experiments were H-17, H-18, and H-26 at 1.12 ppm, 0.68 ppm, and 3.09 ppm, respectively, for TUDCA.

NMR parameters provide information about the interaction processes between ligands and

proteins, such as the selective and non-selective proton relaxation rates analysed with and without albumin. The concentrations were carefully selected, and the solution viscosity did not change with increasing HSA concentration. Table 2 presents the experimental values of R_i^{se} and R_i^{ns} of the H–17, H-18, and H-26 protons for TUDCA in relation to the HSA concentrations. In the absence of HSA, R_i^{ns} was higher than R_i^{se}. This result indicates that TUDCA (without protein) exhibits fast re-orientational motions in solution and the dynamic conditions allow the interaction to be investigated through analysis of the selective and non-selective spin–lattice relaxation rates of the ligand. Meanwhile, R_i^{se} became higher than R_i^{ns} with increasing protein concentration. The selective relaxation rate enhancements reveal the existence of a significant contribution from the bound ligand fraction to the observed relaxation rate, suggesting the presence of an interaction between TUDCA and HSA.

In evaluating the strength of the binding process, the parameter normalized affinity index $\left[A_i^N\right]_L^T$ of the ligand–protein system was determined by calculating the slope of the straight line describing the dependence of the proton selective relaxation rate enhancements on the protein concentration. Fig. 3 shows the results of the linear regression analysis of the normalized selective relaxation enhancements ΔR_{iN}^{se} versus HSA concentration for the H-17, H-18, and H-26 protons of TUDCA. The values of $\left[A_i^N\right]_L^T$ for the H-17 (26404.9 ± 111.8 $L \cdot mol^{-1}$), H-18 (28095.2 ± 105.6 $L \cdot mol^{-1}$), and H-26 (32521.3 ± 117.2 $L \cdot mol^{-1}$) in TUDCA–HSA system were very similar and the small differences may caused by different spin densities. And according to NMR methods above, the complex equilibrium constant *K* was calculated to be 9619.1±19.4 $L \cdot mol^{-1}$ (average of three values). The binding strength may

be obtained to understand the distribution and biological effects of TUDCA as driven by the interaction processes with HSA.

In the meantime, the results obtained by NMR analysis were compared with the equilibrium constant *K* from fluorescence measurements based on the method we reported before.[22] From the Fig. 4, the observed quenching in fluorescence originate from the Trp residue and a remarkable blue shift at the maximum wavelength clearly indicate that TUDCA had a combination effect to HSA and changes in polarity and hydrophobicity around Trp residues. Figure inset shows good linearity of the F_0/F plots for HSA versus quencher concentrations at 25 °C. The obtained quenching constant was 3402.7 $L \cdot mol^{-1}$. The binding constant of bound TUDCA to HSA was determined by plotting the double-logarithm regression curve of the fluorescence data using the modified Stern–Volmer equation and calculated to be 9862.8 $L \cdot mol^{-1}$, which is consistent with the NMR method data. In addition, the emissions of the ternary mixtures of TUDCA, HSA, and warfarin/ibuprofen were measured. The binding constant decreased remarkably in the presence of warfarin, but showed minimal effects in the presence of ibuprofen. TUDCA possibly binds to HSA in subdomain IIA.

To clearly describe the interactions between TUDCA and HSA, the complementary application of the molecular model was applied using AutoDock program package. The AutoDock strategy was used to search over the entire surface of the protein for the binding sites that simultaneously optimize the conformations of the peptides.[2, 40] The aim of the present study is to identify the exact binding site of TUDCA on HSA and promote visual

understanding of the binding site. A total of 11 multimember conformational clusters were gathered from 200 docking runs. From Fig. 5A, the highest populated cluster contained nearly half of the obtained conformations and found to be the lowest on the energy scale. The predicted binding model results of top 5 in this cluster are shown in Table 3. From the values of inhibition constant and binding constants, the most favorable conformation of TUDCA binding with HSA approximated to the NMR experimental values. The optimum interaction between TUDCA and HSA in all runs of docking procedure with the lowest binding energy of –7.91 kcal·mol^{-1} was then used for binding orientation and is shown in Fig. 5B. The 2D ligand interaction diagram is shown in Fig. 5C.

In the optimal binding model, TUDCA was situated within subdomain IIA in Sudlow's site 1 of HSA. A binding pocket was formed to hold the ligand, and the TUDCA molecule was mainly surrounded by Ser202, Phe211, Leu198, Arg218, Lys195, Arg222, His242, Ala291, Lys199, Trp214, and Val344, which are active amino acids for the ligand-HSA interaction. The docking studies provided the inhibition constant of 1.59 μM, and the electrostatic energy of the system was –2.19 kcal·mol^{-1}. In addition, the docked conformation shows that five hydrogen bonds were present in the TUDCA-HSA system. A hydrogen bond was found at 1.992 Å between an oxygen ligand and Trp214, and Arg218 was in a suitable position to form two hydrogen bonds with TUDCA atom with distances of 1.781 and 2.108 Å, respectively. The O atoms of TUDCA formed the other two hydrogen bonds with the H atoms of Arg 222 of the protein (H-bond distances of 1.794 and 2.021 Å). These hydrogen bond networks contributed to the 3D space position change in TUDCA, adapting the shape of the pocket of

Subdomain IIA and stabilizing the docking conformation.

Conclusions

Our study provides fresh insight into the binding patterns and structure-affinity relationship of tauroursodeoxycholic acid with human serum albumin. The NMR parameters and molecule docking studies clearly suggested that TUDCA can strongly bind to HSA in site 1 which were further proved by the fluorescence binding and competitive experiments with consistent results. The determination of the affinity index based on nuclear spin relaxation analysis as a measure of the overall binding behaviour of different drugs and proteins is confirmed to evaluate the strength of the interaction processes. NMR methodology together with docking simulations constitute is a useful approach to confirm the binding mechanism of bioactive ligands to macromolecule receptors.

Acknowledgements

Authors gratefully acknowledge the Analytical & Testing Center of Sichuan University for the assistance on the NMR experiments. We also would like to thank the editors of Enpapers for editing the manuscript.

References

1. C. Kanakis, P. Tarantilis, M. Polissiou, S. Diamantoglou and H. Tajmir-Riahi, *J. Mol. Struct.*, 2006, **798**, 69-74.

2. M. Sarkar, S. S. Paul and K. K. Mukherjea, *J. Lumin.*, 2013, **142**, 220-230.

3. P. Daneshgar, A. A. Moosavi-Movahedi, P. Norouzi, M. R. Ganjali, A. Madadkar-Sobhani and A. A. Saboury, *Int. J. Biol. Macromol.*, 2009, **45**, 129-134.

4. T. Peters Jr, All about albumin: biochemistry, genetics, and medical applications, *Academic press*, 1995.

5. J. Flarakos, K. L. Morand, P.Vouros, *Anal. Chem.* 2005,**77**,1345-1353.

6. A. Crosignani, P. M. Battezzati, K. D. Setchell, P. Invernizzi, G. Covini, M. Zuin and M. Podda, *Digest. Dis. Sci.*, 1996, **41**, 809-815.

7. J. M. Gaspar, A. Martins, R. Cruz, C. M. Rodrigues, A. F. Ambrosio and A. R. Santiago, *Neuroscience*., 2013, **253**, 380-388.

8. B. Nicholson, S. Center, J. Randolph, P. Rowland, M. Thompson, A. Yeager, H. Erb, J. Corbett and D. Watrous, *Res. Vet. Sci.*, 1996, **61**, 258-262.

9. M. Kars, L. Yang, M. F. Gregor, B. S. Mohammed, T. A. Pietka, B. N. Finck, B. W. Patterson, J. D. Horton, B. Mittendorfer and G. S. Hotamisligil, *Diabetes*, 2010, **59**, 1899-1905.

10. C. M. Rodrigues, S. Solá, Z. Nan, R. E. Castro, P. S. Ribeiro, W. C. Low and C. J. Steer, *P. Natl. Acad. Sci.*, 2003, **100**, 6087-6092.

11. N. Wang, Y. Feng, F. Cheung, O. Y. Chow, X. Wang, W. Su and Y. Tong, *BMC Complem. Altern. M*., 2012, **12**, 239.

12. I. H. Park, M. K. Kim and S. U. Kim, *Biochem. Bioph. Res. Co.*, 2008, **377**, 1025-1030.

13. L. Ozcan, A. S. Ergin, A. Lu, J. Chung, S. Sarkar, D. Nie, M. G. Myers Jr and U. Ozcan, *Cell Metab.*, 2009, **9**, 35-51.

14. S. S. Cao and R. J. Kaufman, *Curr. Biol*., 2012, 22, R622-R626.

15. G. W. MOLL JR and R. L. ROSENFIELD, *J. Clin. Endocr. Metab.*, 1978, **46**, 501-503.

16. M. H. Rahman, T. Maruyama, T. Okada, K. Yamasaki and M. Otagiri, *Biochem. Pharmacol.*, 1993, **46**, 1721-1731.

17. A. Saboury, *J. Iran. Chem. Soc.*, 2006, 3, 1-21.

18. Y. Zhang, J. H. Li, Y. S. Ge, X. R. Liu, F. L. Jiang and Y. Liu, *J. Fluoresc.*, 2011, **21**, 475-485.

19. X. Zhu, Y. Ding, B. Lin, A. Jakob and B. Koppenhoefer, *Electrophoresis*, 1999, **20**, 1869-1877.

20. N. Sisavath, L. Leclercq, T. Le Saux, F. Oukacine and H. Cottet, *J. Chromatogr.*, 2013, **1289**, 127-132.

21. R. Thakur, A. Das and A. Chakraborty, *Rsc Adv.*, 2014, **4**, 14335-14347.

22. D. Wu, J. Yan, J. Wang, Q. Wang and H. Li, *Food Chem.*, 2015. **170**, 423–429.

23. S. Tabassum, W. M. Al-Asbahy, M. Afzal and F. Arjmand, *J. Photoch. Photobio. B*, 2012, **114**, 132-139.

24. S. Tunç, O. Duman, İ. Soylu and B. Kancı Bozoğlan, *J. Hazard. Mater.,* 2014, **273**, 36-43.

25. D. Xiao, L. Zhang, Q. Wang, X. Lin, J. Sun and H. Li, *J. Lumin.*, 2014, **146**, 218-225.

26. C. Bonechi, S. Martini and C. Rossi, *Med. Chem. Lett.*, 2009, **17**, 1630-1635.

27. A. Jana, K. T. Nguyen, X. Li, P. Zhu, N. S. Tan, H. Ågren and Y. Zhao, *ACS Nano*, 2014.

28. R. Freeman, H. Hill, B. Tomlinson and L. Hall, *The J. Chem. Phys.*, 1974, **61**, 4466-4473.

29. D. Neuhaus and M. P. Williamson, The nuclear Overhauser effect in structural and conformational analysis, *VCH New York*, 1989.

30. M. Delfini, R. Gianferri, V. Dubbini, C. Manetti, E. Gaggelli and G. Valensin, *J. Magn. Reson.*, 2000, **144**, 129-133.

31. M. Rozga, M. Kloniecki, A. Jablonowska, M. Dandlez and W. Bal, *Biochem. Bioph. Res. Co.*, 2007, **364**, 714-718.

32. C. Bonechi, S. Martini and C. Rossi, *J. Mater. Sci.*, 2011, **46**, 2541-2547.

33. C. Rossi, A. Donati, C. Bonechi, G. Corbini, R. Rappuoli, E. Dreassi and P. Corti, *Chem. Phys. Lett.*, 1997, **264**, 205-209.

34. C. Rossi, C. Bonechi, S. Martini, M. Ricci, G. Corbini, P. Corti and A. Donati, *Magn. Reson. Chem.*, 2001, **39**, 457-462.

35. S. Martini, C. Bonechi, M. Casolaro, G. Corbini and C. Rossi, *Biochem. Pharmacol.*, 2006, **71**, 858-864.

36. S. Martini, C. Bonechi and C. Rossi, *J. Nat. Prod.*, 2008, **71**, 175-178.

37. E. Gaggelli, G. Valensin, T. Kushnir and G. Navon, *Magn. Reson. Chem.*, 1992, **30**, 461-465.

38. G. B. Rocha, R. O. Freire, A. M. Simas and J. J. Stewart, *J. Comput. Chem.*, 2006, **27**, 1101-1111.

39. O. B. Ijare, B. S. Somashekar, Y. Jadegoud, and G. A. Nagana Gowda, *Lipids*, 2005, **40** 1031-1041.

40. G. M. Morris, R. Huey, W. Lindstrom, M. F. Sanner, R. K. Belew, D. S. Goodsell and A. J. Olson, *J. Comput. Chem.*, 2009, **30**, 2785-2791.

Table 1

^{1}H chemical shifts of TUDCA in D_2O solution (pH 7.4) at 25 °C

No.	Type	Proton σ [ppm]	
		α	β
1	CH_2	1.80	1.06
2	CH_2	1.26	1.64
3	CH	---	3.62
4	CH_2	1.64	1.54
5	CH	---	1.54
6	CH_2	1.58	1.75
7	CH	3.62	---
8	CH	---	1.46
9	CH	1.46	---
10	C	---	
11	CH_2	1.46	1.36
12	CH_2	1.24	2.03
13	C	---	
14	CH	1.33	---
15	CH_2	1.84	1.42
16	CH_2	1.89	1.36
17	CH	1.12	---
18	CH_3	0.68	
19	CH_3	0.94	
20	CH	1.42	
21	CH_3	0.94	
22	CH_2	1.38, 1.80	
23	CH_2	2.31, 2.19	
24	C	---	
25	CH_2	3.57	
26	CH_2	3.09	

Table 2

R_i^{se} and R_i^{ns} values of H-17,H-18, H-26 protons for TUDCA (4.0 mM) in the presence of variable HSA concentrations at 25 °C.

HSA concentration (μM)	R_i^{se} (s^{-1}) H-17	R_i^{ns} (s^{-1}) H-17	R_i^{se} (s^{-1}) H-18	R_i^{ns} (s^{-1}) H-18	R_i^{se} (s^{-1}) H-26	R_i^{ns} (s^{-1}) H-26
0	1.24±0.03	1.31±0.02	0.67±0.03	0.80±0.02	0.95±0.02	1.09±0.04
3.0	1.33±0.02	1.32±0.03	0.78±0.02	0.76±0.01	1.09±0.05	1.07±0.06
6.0	1.41±0.05	1.28±0.04	0.85±0.03	0.81±0.02	1.15±0.02	1.11±0.01
9.0	1.46±0.03	1.27±0.01	0.93±0.04	0.78±0.02	1.26±0.04	1.06±0.02
12	1.53±0.01	1.32±0.02	1.02±0.01	0.83±0.04	1.39±0.03	1.04±0.04
15	1.60±0.04	1.34±0.03	1.10±0.06	0.85±0.01	1.48±0.01	1.08±0.01

Table 3

Docking summary of HSA with TUDCA in the highest populated cluster by AutoDock program generating different ligand conformers (Top 5).

Sub rank	Binding energy ($kcal \cdot mol^{-1}$)	Electrostatic energy ($kcal \cdot mol^{-1}$)	Inhibition constant (μmol)	Association constant ($10^3\ L \cdot mol^{-1}$)	Number of H-bonds	Cluster rmsd	Reference rmsd
1	-7.91	-2.19	1.59	10.10	5	0.00	29.27
2	-7.64	-2.35	2.49	9.87	4	1.25	29.74
3	-7.63	-1.9	2.55	9.81	4	1.81	29.30
4	-7.59	-2.81	2.73	9.69	6	1.78	29.54
5	-7.53	-2.44	3.02	9.52	5	1.67	29.38

Figure Captions:

Fig. 1. Chemical structure of TUDCA.

Fig.2. 400 MHz ^{1}H NMR proton spectrum of 4.0 mM TUDCA in D_2O solution at 25 °C.

Fig. 3. Linear regression analysis of H–17, H-18, and H-26 normalized selective relaxation enhancement ΔR_{iN}^{se} as a function of albumin concentration of TUDCA solution. Normalized affinity index values $\left[A_i^N\right]_L^T$ are also reported with corresponding errors.

Fig. 4. Fluorescence spectra of HSA in the presence of TUDCA: c(HSA)=2.0×10^{-6} mol·L^{-1}, c(TUDCA)=1.0, 2.0, 3.0, 4.0, 5.0, and 6.0×10^{-5} mol·L^{-1}. Curve below shows the emission spectrum of 2.0×10^{-6} mol·L^{-1} TUDCA only. Stern–Volmer plot for HSA fluorescence quenching caused by TUDCA at 25 °C (inset).

Fig. 5. (A) Cluster analyses of the AutoDock docking runs of TUDCA-HSA system. (B) Portrait of optimal TUDCA–HSA conformation generated by AutoDock Version 4.2.5.1. (C) Schematic diagram obtained using the 2D diagram feature of Accelrys Discovery Studio 3.1 showing interactions between TUDCA and its neighboring residues. Pink circles represent residues participating in hydrogen bonds, charge, or polar interactions. Green circles are residues participating in van der Waals interactions. A light blue circle surrounding a given residue/atom denotes its solvent-accessible surface.

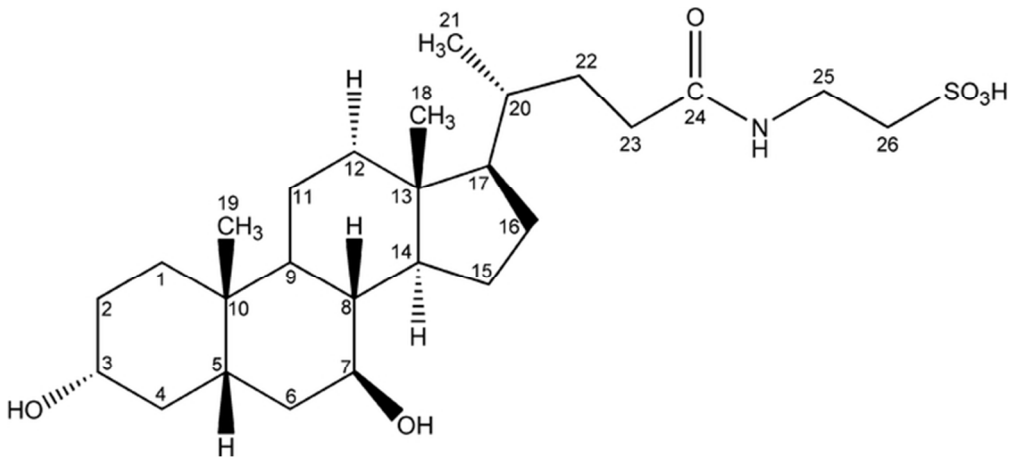

Figure 1
60x27mm (300 x 300 DPI)

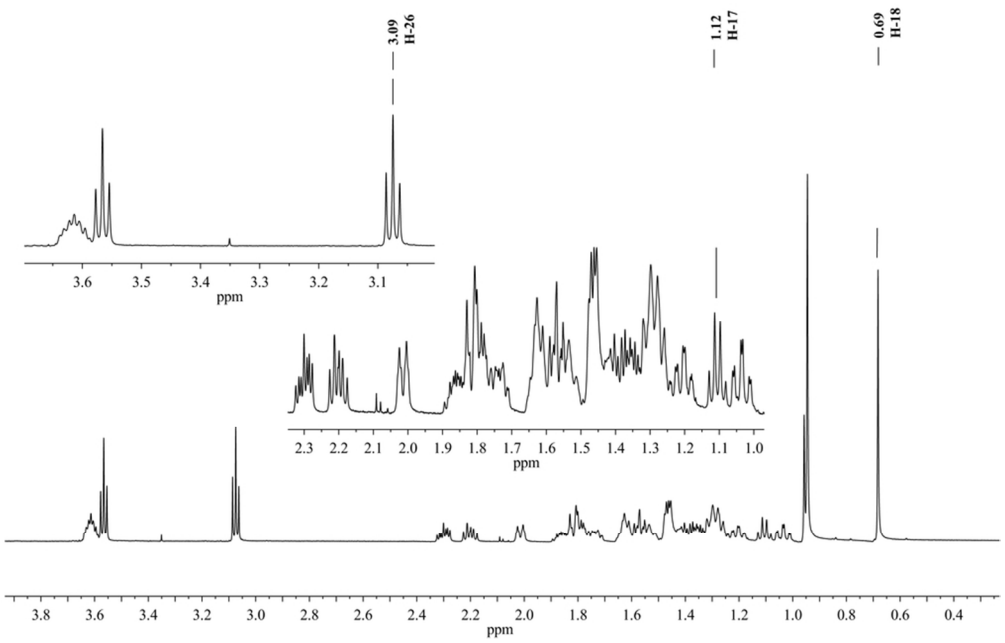

Figure 2
85x54mm (300 x 300 DPI)

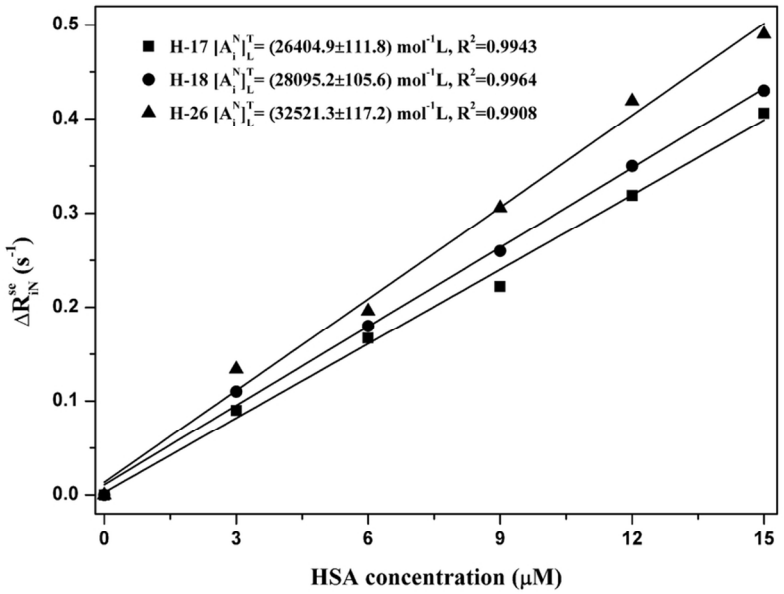

Figure 3
95x67mm (300 x 300 DPI)

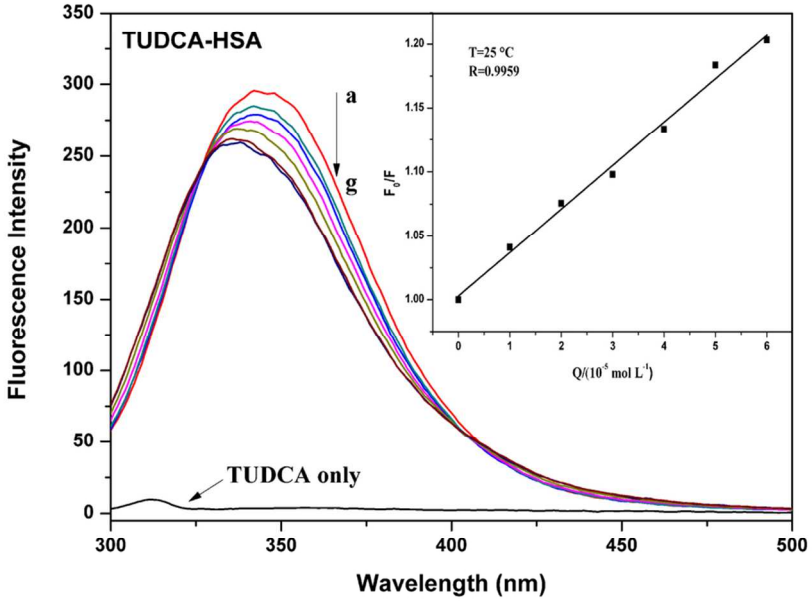

Figure 4
95x67mm (300 x 300 DPI)

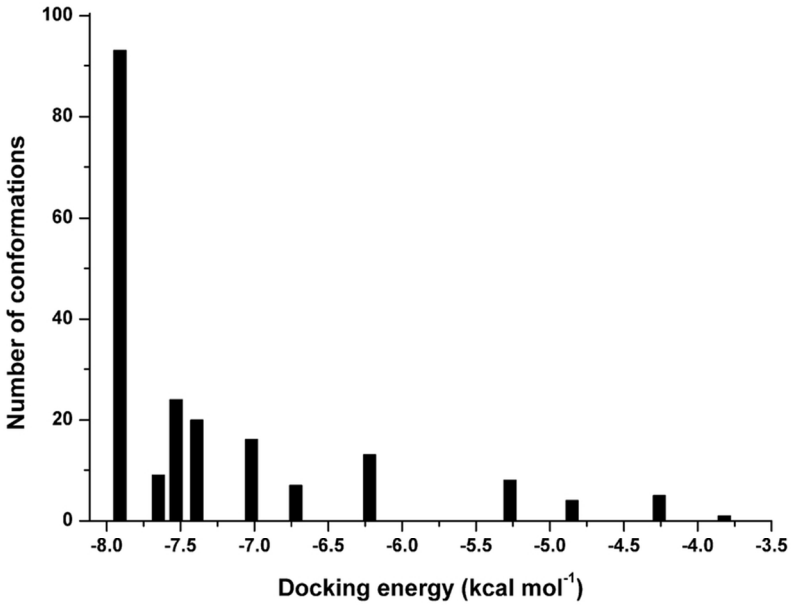

Figure 5A
95x67mm (300 x 300 DPI)

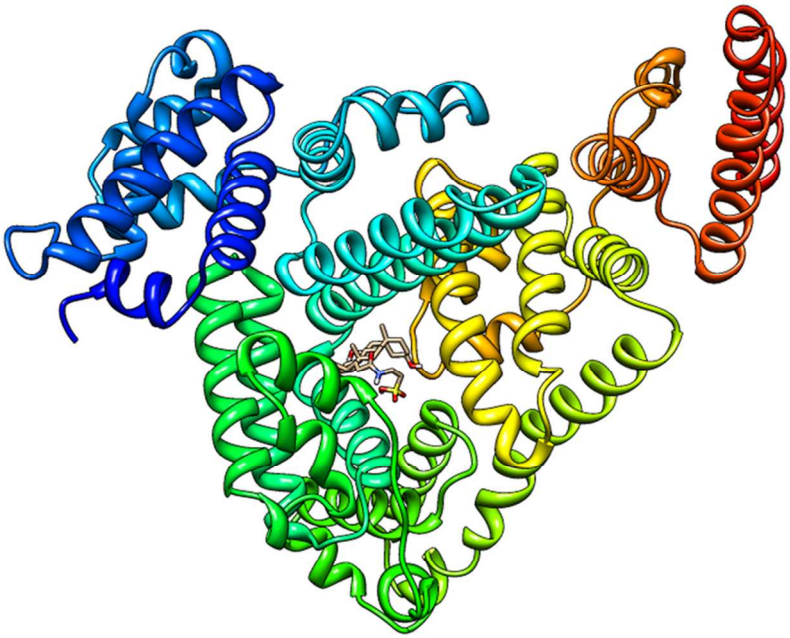

Figure 5B
90x60mm (300 x 300 DPI)

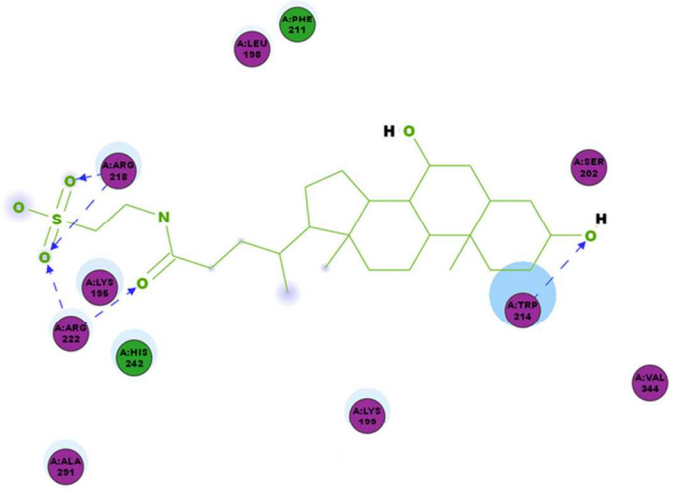

Figure 5C
81x49mm (300 x 300 DPI)